NOTES AND CORRESPONDENCE

Detecting Propagating Signals with Complex Empirical Orthogonal Functions: A Cautionary Note

M. A. MERRIFIELD† AND R. T. GUZA

Center for Coastal Studies, Scripps Institution of Oceanography, La Jolla, California

28 November 1989 and 8 February 1990

ABSTRACT

A limitation on the performance of complex empirical orthogonal function (CEOF) analysis in the time domain is illustrated with synthetic, noise-free, nondispersive, propagating signals. Numerical examples using a band-limited white spectrum and a simulation of costal-trapped waves sampled with an array of tide gauges, demonstrate that CEOF analysis is degraded with increasing $\Delta\kappa\Delta X$ ($\Delta\kappa$ is the wavenumber bandwidth and ΔX is the instrument array length). A relatively wide wavenumber bandwidth [$\Delta\kappa\Delta X > o(2\pi)$] results in a significant loss of variance recovery towards the ends of the array. The CEOF method does yield an average frequency and wavenumber for the first mode, independent of $\Delta\kappa\Delta X$, that accurately estimate the phase speed of the nondispersive propagating signal. These simple simulations indicate that modal spatial patterns from a time domain CEOF analysis of wide-banded signals should be interpreted cautiously.

1. Introduction

Empirical orthogonal functions (EOFs, Lorenz 1956), a standard technique for describing coherent variability in geophysical data, give the most efficient description of the observed variability, often reducing large datasets to a few dominant modes. These dominant empirical modes are sometimes useful in representing dynamical modes in the data (e.g., Kundu et al. 1975), although the requirement of orthogonality in both time and space, the use of the covariance (or correlation) matrix at zero lag to describe the variability, and the particular sampling of the observed field require careful consideration before assigning any physical significance to a given mode. In particular, the use of the zero-lagged covariance matrix limits the analysis to the detection of patterns that are in phase or π out of phase over the array.

An alternative method for detecting propagating patterns is complex empirical orthogonal function analysis in either the frequency (Brillinger 1975) or time domains (Rasmusson et al. 1983). The former obtains principal components from the cross-spectral matrix, while the latter, termed CEOFs[1] in the present note following Barnett (1983), obtains principal components and temporal expansions from an essentially "wide-banded" cross-spectral matrix. The advantages of performing CEOF analysis in the time domain are that problems associated with spectral estimation are (apparently) avoided, phase speeds may be computed in a straightforward manner, and time series reconstruction from the CEOF modes provides a convenient means for determining the temporal nature of the propagating signal. Time domain analysis has been used to detect large-scale traveling patterns in meteorologic (Barnett 1983; and others) and oceanographic observations (White and Tabata 1987; and others). Horel (1984) has presented several examples of CEOF analysis on synthetic time series. In his example 4, a geophysical dataset is simulated as short-duration irregularly occurring progressive waves traveling through a square grid of sensors. The CEOF analysis is unable to isolate this propagating variability in a single mode and Horel concludes, "one should not expect to be able to detect slow moving, irregularly spaced pulses over vast distances accurately on the basis of complex correlations."

Here, we expand on Horel's result by identifying the nondimensional parameter that causes the spread of propagating variability into more than one CEOF mode. The discussion is limited to nondispersive waves for which the analysis is best suited since, typically, a single phase speed is estimated for each mode. The present note is motivated by an unsuccessful attempt to use time domain CEOFs in a study of coastal-trapped waves observed in coastal sea level and moored observations along the Mexican Pacific coast (Merrifield and Winant 1990). Tests of CEOF performance include both band-limited, white spectra and a simulation of

† Present address: School of Mathematics, University of New South Wales, Kensington, NSW, Australia.

[1] The term *complex empirical orthogonal decomposition* has also been used by Kundu and Allen (1976) for EOFs of true vector time series, e.g. current or wind velocity, and should not be confused with the present method.

Corresponding author address: Dr. Mark A. Merrifield, Mathematics Oceanography Laboratory, The University of New South Wales, P.O. Box 1, Kensington, New South Wales, Australia 2033.

the coastal-trapped wave observations. These simple examples show that CEOF analysis is not appropriate for nondispersive processes that are broad-banded in wavenumber ($\Delta\kappa$) relative to the array size (ΔX). Although the relevance of the parameter $\Delta\kappa\Delta X$ is perhaps intuitively obvious and also follows from standard analysis of the coherence of wave phenomena, we feel that this limitation of the CEOF method has not been universally appreciated and can lead to erroneous interpretation of modal spatial patterns. The results are also relevant to frequency domain EOFs; however, we emphasize the time domain analysis because wavenumber bandwidths tend to be inherently large.

2. The method

The time domain CEOF method obtains phase information about a scalar field without explicitly resorting to a spectral analysis. Following Barnett (1983) and Horel (1984), a scalar field $u_j(t)$, where j signifies spatial position ($j = 1, 2, \cdots, N$) and t is time, is represented in the usual Fourier sense as

$$u_j(t) = \sum_{\omega} [a_j(\omega)\cos(\omega t) + b_j(\omega)\sin(\omega t)]. \quad (1)$$

To obtain phase information between stations, a complex representation of $u_j(t)$ is invoked:

$$U_j(t) = \sum_{\omega} c_j(\omega)e^{-i\omega t}, \quad (2)$$

where $c_j(\omega) = a_j(\omega) + ib_j(\omega)$. Then $U_j(t)$ can be written in the form

$$\begin{aligned} U_j(t) &= \sum_{\omega} \{[a_j(\omega)\cos(\omega t) + b_j(\omega)\sin(\omega t)] \\ &\quad + i[b_j(\omega)\cos(\omega t) - a_j(\omega)\sin(\omega t)]\} \\ &= u_j(t) + i\hat{u}_j(t). \end{aligned} \quad (3)$$

The real part of $U_j(t)$ is the original scalar field. The imaginary part is the quadrature function of $u_j(t)$, or the Hilbert transform (Thomas 1969), which is equivalent to phase shifting each spectral component of $u_j(t)$ by $\pi/2$. In this study, $\hat{u}$ is obtained from the Fourier coefficients.

The covariance matrix of $U_j(t)$ is

$$C_{jk} = \langle U_j^*(t)U_k(t)\rangle_t \quad (4)$$

where $\langle \ldots \rangle_t$ denotes time averaging. It follows from standard spectral analysis theory that

$$C_{jk} = \int_0^{\omega_n} \phi_{jk}(\omega)d\omega, \quad (5)$$

where ϕ_{jk} is the cross spectrum and ω_n is the Nyquist frequency. The CEOF analysis in the time domain obtains the eigenfunctions of C and is, thus, equivalent to a frequency domain EOF with the cross-spectrum integrated over all frequencies.

As in a standard EOF analysis, the eigenfunctions $B_n(x)$, where n denotes mode number, are obtained from C, and the temporal expansions are given by

$$A_n(t) = \sum_{j=1}^{N} U_j(t)B_n(x). \quad (6)$$

In a CEOF analysis, however, both $B_n(x)$ and $A_n(t)$ are complex. The complex time series can then be represented as

$$U_j(t) = \sum_{n=1}^{N} A_n(t)B_n^*(x). \quad (7)$$

A spatial and temporal phase are defined as

$$\theta_n(x) = -\tan^{-1}[\mathrm{Im}B_n(x)/\mathrm{Re}B_n(x)], \quad (8a)$$

$$\phi_n(t) = \tan^{-1}[\mathrm{Im}A_n(t)/\mathrm{Re}A_n(t)], \quad (8b)$$

with a wavenumber, frequency and phase speed for each mode given by

$$\kappa_n = d\theta_n/dx \quad (9a)$$

$$\omega_n = d\phi_n/dt \quad (9b)$$

$$c_n = \omega_n/\kappa_n. \quad (10)$$

3. Test cases

a. *Band-limited white spectra*

A nondispersive plane wave propagating at phase speed c past an array of sensors at positions j is given by

$$\begin{aligned} u_j(t) &= \sum_{\omega} [\alpha(\omega)\cos(\kappa x_j - \omega t) \\ &\quad + \beta(\omega)\sin(\kappa x_j - \omega t)] \\ &= \sum_{\omega} [a_j(\omega)\cos(\omega t) + b_j(\omega)\sin(\omega t)], \end{aligned} \quad (11)$$

where $\kappa = \omega/c$, and

$$\begin{aligned} a_j(\omega) &= \alpha(\omega)\cos(\kappa x_j) + \beta(\omega)\sin(\kappa x_j) \\ b_j(\omega) &= \alpha(\omega)\sin(\kappa x_j) - \beta(\omega)\cos(\kappa x_j). \end{aligned} \quad (12)$$

For this example, $u_j(t)$ is a white, band-limited signal given by

$$\alpha(\omega)^2 + \beta(\omega)^2 = \begin{cases} A^2, & \text{if } \omega_1 \leqslant \omega \leqslant \omega_2 \\ 0, & \text{if } \omega > \omega_2, \omega < \omega_1. \end{cases} \quad (13)$$

Substitution of Eq. (2) into (4) yields

$$C_{jk} = \sum_{\omega} [a_j a_k + b_j b_k + i(a_j b_k - b_j a_k)], \quad (14)$$

and using Eqs. (12) and (13) gives

$$C_{jk} = A^2 \sum_{\omega=\omega_1}^{\omega_2} e^{-i\kappa(\omega)\Delta x_{jk}}, \quad (15)$$

where $\Delta x_{jk} = x_j - x_k$. Replacing the summation in (15) with an integral gives

$$C_{jk} \approx A^2 T(2\pi)^{-1} \int_{\omega_1}^{\omega_2} e^{-i\kappa(\omega)\Delta x_{jk}} d\omega$$

$$= A^2 M \operatorname{sinc}(\Delta\kappa \Delta x_{jk}/2) e^{-i\bar{\kappa}\Delta x_{jk}} \quad (16)$$

where $\Delta\kappa = \kappa(\omega_2) - \kappa(\omega_1)$, $\bar{\kappa} = (\kappa(\omega_2) + \kappa(\omega_1))/2$, $M = (\omega_2 - \omega_1)T/2\pi$, $\operatorname{sinc}(y) \equiv \sin(y)/y$.

We could not determine a general algebraic expression for the eigenvalues and eigenfulctions of C for an arbitrary number of sensors (N). The case of two sensors, however, illustrates some important properties of C. The eigenvalues and eigenfunctions are given by

$$\lambda_{1,2} = A^2 M[1 \pm |\operatorname{sinc}(\Delta\kappa \Delta x/2)|],$$

$$B_{1,2} = (e^{-i\bar{\kappa}x_1}, \pm e^{-i\bar{\kappa}x_2}). \quad (17)$$

Note that the performance of the CEOF analysis, as measured by the percentage of variance explained in mode 1, depends on the spread in wavenumber relative to the array size; as the parameter $\Delta\kappa\Delta x$ decreases, more of the variance is contained in the lowest CEOF mode (Fig. 1a). The mode 1 wavenumber, determined from Eqs. (8) and (9), is $\bar{\kappa}$, the average wavenumber of the band.

CEOFs of similar white, band-limited signals, but sampled with arrays of $N = 4$, 6, 10 and 20 equally spaced sensors over a fixed total array length (ΔX), were computed numerically. For each value of N, 100 test runs are made by varying the phase speed and the frequency bandwidth (ω_1, ω_2) of the wave signal, thus fixing the wavenumber bandwidth and $\Delta\kappa\Delta X$. The percentage of the total variance explained by mode 1, as a function of $\Delta\kappa\Delta X$, is similar for all values of N (Fig. 1a); it decays monotonically for $\Delta\kappa\Delta X < 2(N - 1)\pi$ and decays asymptotically to $100/N$, the re-

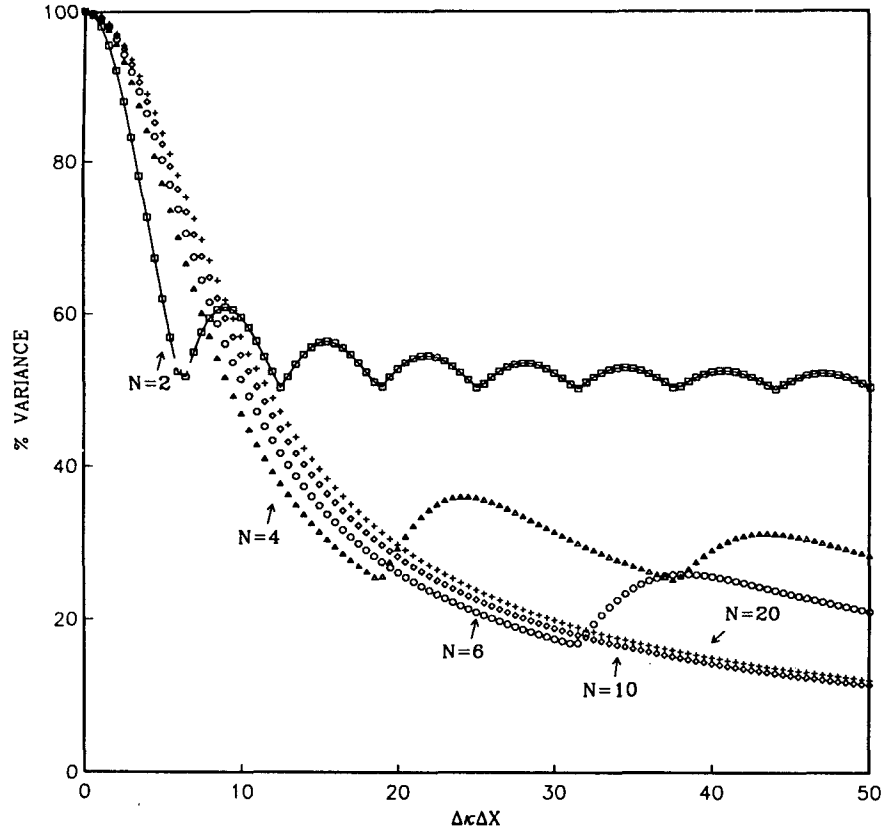

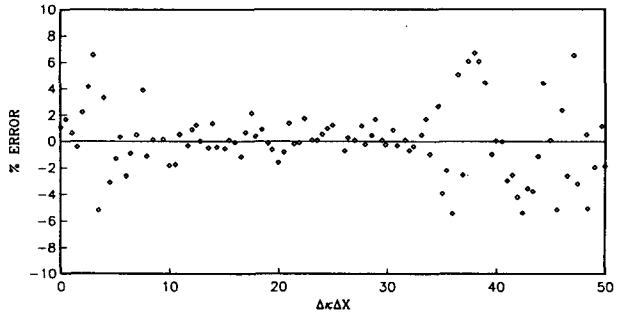

FIG. 1a. The total variance explained by mode 1 as a function of $\Delta\kappa\Delta X$, the product of the wavenumber bandwidth and the total array length, for band-limited, white spectra and various numbers of sensors (N). The solid line is the analytic function for $N = 2$ [see Eq. (17)].

FIG. 1b. The error between the true and mode 1 phase speeds versus $\Delta\kappa\Delta X$ for band-limited, white spectra and 10 sensors.

covered variance of one sensor, for $\Delta\kappa\Delta X > 2(N-1)\pi$. For each test run, the mode 1 spatial and temporal phases (8) correspond approximately to the average wavenumber and frequency of the spectral band, and the true phase speed of the propagating signal (10) is always recovered in mode 1 to within 5% accuracy (see Fig. 1b for $N = 10$).

The percentage of variance explained at each spatial position by mode 1 (Fig. 2) shows that the decrease in mode 1 total variance is due to the poor recovery of the signal towards the ends of the spatial array. The importance of the parameter $\Delta\kappa\Delta X$ in explaining the variability is analogous to the importance of phase wobble when computing the coherence in a spectral band. The more the phase varies over a band, the lower the coherence for that band. In the expression for C (16), $\kappa\Delta x_{jk}$ is the phase analog and $\Delta\kappa\Delta x_{jk}$ is the phase spread between any two sensors. Thus, as $\Delta\kappa\Delta x_{jk}$ increases, C_{jk} decreases. The CEOF maximizes the variability in mode 1 by minimizing the Δx_{jk}, i.e. by choosing the maximum of the spatial amplitude in the middle of the array. Note $\Delta\kappa\Delta X$ is a measure of the largest range in phase computed over the array (between the two furthest sensors) and $\Delta\kappa\Delta X/(N-1)$ is the minimum phase range (between adjacent sensors). When $\Delta\kappa\Delta X = 2(N-1)\pi$, the coherence between adjacent sensors [separation $\Delta X/(N-1)$] is zero [Eq. (16)], and total recovered variance has a local minimum (Fig. 1a). For $\Delta\kappa\Delta X \gg 2(N-1)\pi$, all sensor pairs are incoherent.

When $\Delta\kappa\Delta X \approx \pi$, waves near the ends of the wavenumber band are approximately in antiphase at the ends of the array and the variance recovered is reduced significantly (Fig. 2). When $\Delta\kappa\Delta X = 2\pi$, the total recovered variance in the case of the band-limited spectrum is reduced to approximately 50%–80% (depending on the number of sensors, Fig. 1a), and $\Delta\kappa\Delta X \leqslant o(2\pi)$ is taken as an approximate constraint on the CEOF analysis for a band-limited, white spectrum.

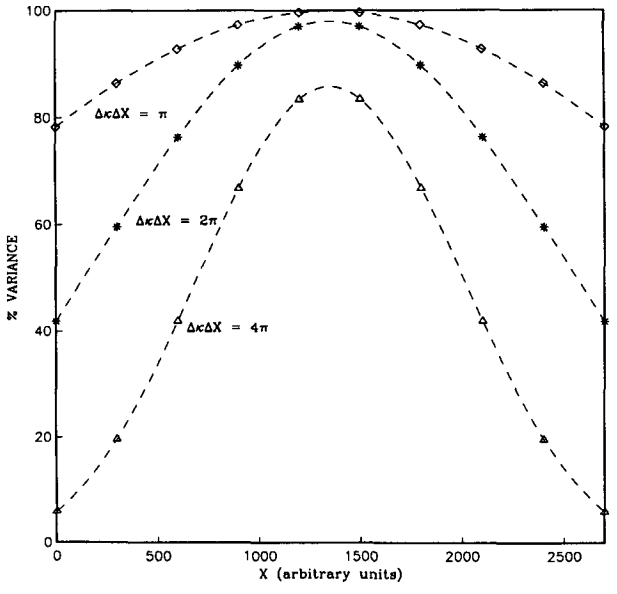

FIG. 2. The percent variance explained by mode 1 at each x position in the array (10 sensors) for band-limited, white spectra and three values of $\Delta\kappa\Delta X$.

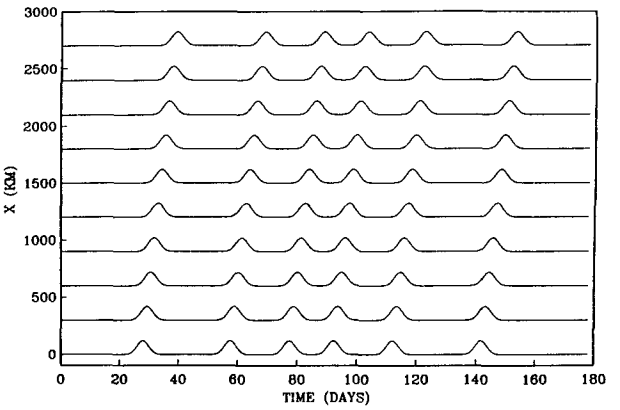

FIG. 3a. Time series of the propagating Gaussian-shaped wave test case at 10 sensor locations.

b. *Propagating Gaussian-shaped wave pulses*

The coastal-trapped wave test case (Fig. 3) consists of a series of irregularly spaced Gaussian-shaped pulses that propagate nondispersively past a one-dimensional, ten-station array. The time series schematically represent coastal sea level observations during one tropical storm season (6 months), at equally spaced stations over a 2700 km distance along the Mexican coast. Wave events last for roughly 10 days, have constant amplitude, and 215 km d^{-1} phase speed. In contrast to the band-limited white spectrum, the wave signal here has a distinctive temporal behavior that we seek to recover by reconstructing the time series with the CEOF mode 1. The autospectrum for the Gaussian wave train is red (Fig. 3b) with a nominal frequency bandwidth of 0.02–0.10 cpd (approximately the half-power points), yielding $\Delta\kappa\Delta X \approx 6$.

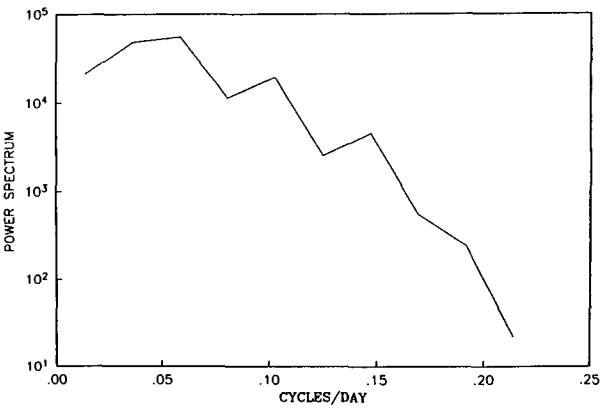

FIG. 3b. The autospectrum of the Gaussian-shaped wave time series.

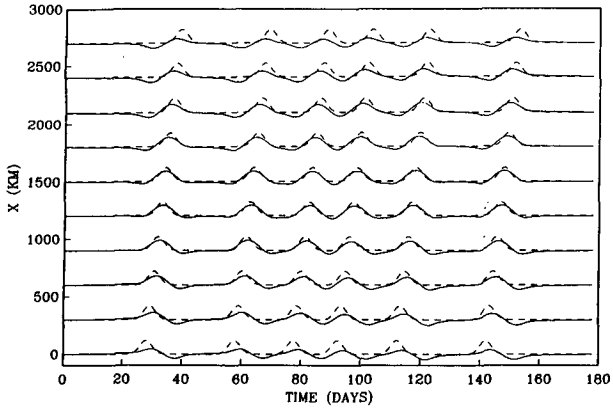

FIG. 4a. The mode 1 reconstructed time series for the propagating Gaussian-shaped wave test case. The dashed lines are the original time series.

As in the previous test case, the CEOF analysis is unable to isolate all of the variability in a single mode. The first mode, describing 66% of the total variance, is used to reconstruct the time series at each station (Fig. 4a). The wave field is only partially accounted for by mode 1, with the percentage of variance described at each station decreasing towards the ends of the array (Fig. 5), similar to Fig. 2. The true phase speed is represented in mode 1 to within 5%.

The application of CEOF analysis on band-passed time series improves the reproduction of the time series by reducing the wavenumber bandwidth of the signal. In this test run, the same wave signal is analyzed, however, in four different frequency bands (0.0–0.05, 0.05–0.1, 0.1–0.15, 0.15–0.2 cpd). This corresponds to reducing the wavenumber bandwidth by very roughly a factor of 2. The low energy portions of a red spectra do not contribute much to the cross-spectrum, so the effective wavenumber is less than for a white spectrum. Again the correct nondispersive phase speed is obtained for each band. When the mode 1 reconstructed time series for each band are summed together at each station, yielding a single broadbanded time domain pattern, the reconstructed and original time series are now in much better agreement (Figs. 4b, 5).

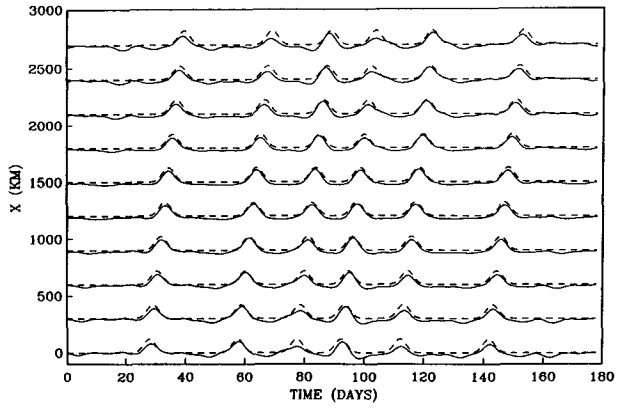

FIG. 4b. The same as Fig. 4a except the time series are first band-passed filtered, CEOFs are obtained for each band, and the mode 1 reconstructed time series in each band are then summed together.

Wavenumber bandwidth effects are, of course, a problem for frequency as well as time domain EOFs. In either case, the usual trade-off occurs in selecting the bandwidth: if the band is too narrow, statistical uncertainty arises in the estimate of the covariance matrix C; if the band is too broad relative to the array length, a single EOF mode is unable to resolve the variability toward the ends of the array. Statistical reliability may be gained by prewhitening across each band prior to forming C (cf. Davis and Bogden 1988) but at the cost of increased effective bandwidth (for fixed bandwidth, the effective bandwidth is maximum for a white spectrum). If the spectrum in Fig. 3b is prewhitened over the four frequency bands, less of the total variance is explained in the sum of the mode 1 reconstructed time series (50% compared to 85% without prewhitening).

4. Summary

Examples using synthetic, noise-free data indicate that complex empirical orthogonal function analysis in the time domain does not isolate, in a single mode, nondispersive propagating signals that are widebanded in wavenumber relative to the instrument array size [$\Delta\kappa\Delta X > o(2\pi)$]. The symptom of broadbandedness is reduced mode 1 signal toward the ends of the spatial array, a feature also observed by Horel (1983). The method does accurately recover an average frequency and wavenumber and, thus, an accurate estimate of phase speed for nondispersive waves, independent of $\Delta\kappa\Delta X$.

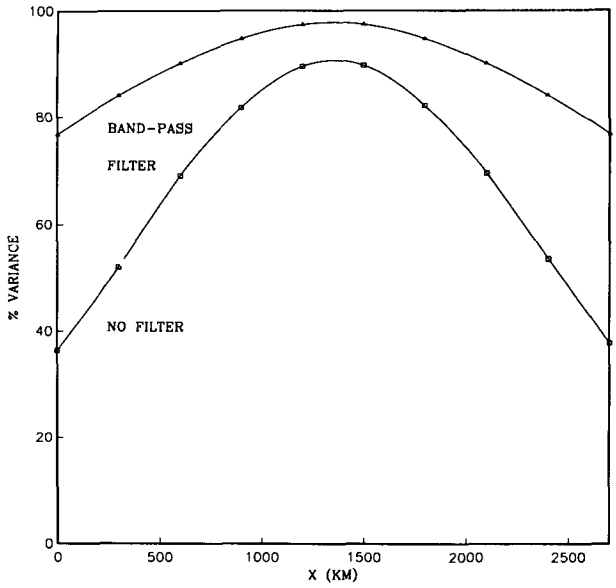

FIG. 5. The percent variance explained at each x position from the time series in Fig. 4.

In practice, the wavenumber bandwidth of the analysis is usually fixed by the duration of the time series and the averaging needed for statistical stability. Because the cross-spectrum between relatively distant sensors is degraded, the ability of the CEOF method to detect large-scale propagating patterns is not increased by lengthening the array beyond the *effective* array length (ΔX_e) determined by the wavenumber bandwidth,

$$\Delta X_e \approx 2\pi/\Delta\kappa.$$

On the other hand, the array should be long enough to resolve a typical wavenumber ($\bar{\kappa}$), spanning a minimum of one wavelength,

$$\Delta X_e \geq 2\pi/\bar{\kappa}.$$

These two constraints show that

$$\Delta\kappa \leq \bar{\kappa}$$

is required for both minimally acceptable resolution and an un-degraded cross-spectral matrix.

Our principal result is that time domain CEOFs are a fairly robust method for estimating the phase speed of nondispersive waves propagating through large arrays. CEOF spatial patterns, however, should be interpreted cautiously; we believe finite bandwidth effects have not been accounted for in some published instances.

Acknowledgments. This work was supported by the Coastal Sciences Branch of the Office of Naval Research, Contract N00014-87-K-0005. Anonymous reviewers made useful comments.

REFERENCES

Barnett, T. P., 1983: Interaction of the monsoon and Pacific trade wind system at interannual time scales. Part 1: The equatorial zone. *Mon. Wea. Rev.*, **111,** 756–773.

Brillinger, D. R., 1975: *Time Series. Data Analysis and Theory,* Holt, Rinehart and Winston.

Horel, J. D., 1984: Complex principal component analysis: Theory and examples. *Climate Appl. Meteor.*, **23,** 1660–1673.

Kundu, P. K., and J. S. Allen, 1976: Some three-dimensional characteristics of low-frequency current fluctuations near the Oregon coast. *J. Phys. Oceanogr.*, **6,** 181–199.

——, —— and R. L. Smith, 1975: Modal decomposition of the velocity field near the Oregon coast. *J. Phys. Oceanogr.*, **5,** 683–704.

Lorenz, E., 1956: Empirical orthogonal function and statistical weather prediction. Rep. No. 1, Statistical Forecasting Program, Dept. of Meteor., Massachusetts Institute of Technology, 44 pp.

Merrifield, M. A., and C. D. Winant, 1989: Shelf circulation in the Gulf of California: A description of the variability. *J. Geophys. Res.*, **94,** 18 133–18 160.

Rasmusson, E. M., P. A. Arkin, W. Y. Chen and J. B. Jalickee, 1981: Bienniel variations in surface temperature over the United States as revealed by singular decomposition. *Mon. Wea. Rev.*, **109,** 181–192.

Thomas, J. B., 1969: *An Introduction to Statistical Communication Theory,* Wiley, 663 pp.

White, W. B., and S. Tabata, 1987: Interannual westward-propagating baroclinic long-wave activity on line P in the eastern midlatitude North Pacific. *J. Phys. Oceanogr.*, **17,** 385–396.